

Reliability implications of partial shading on CIGS photovoltaic devices

A literature review

Bakker, Klaas; Weeber, Arthur; Theelen, Mirjam

DOI

[10.1557/jmr.2019.373](https://doi.org/10.1557/jmr.2019.373)

Publication date

2019

Document Version

Final published version

Published in

Journal of Materials Research

Citation (APA)

Bakker, K., Weeber, A., & Theelen, M. (2019). Reliability implications of partial shading on CIGS photovoltaic devices: A literature review. *Journal of Materials Research*, 34(24), 3977-3987. <https://doi.org/10.1557/jmr.2019.373>

Important note

To cite this publication, please use the final published version (if applicable). Please check the document version above.

Copyright

Other than for strictly personal use, it is not permitted to download, forward or distribute the text or part of it, without the consent of the author(s) and/or copyright holder(s), unless the work is under an open content license such as Creative Commons.

Takedown policy

Please contact us and provide details if you believe this document breaches copyrights. We will remove access to the work immediately and investigate your claim.

Reliability implications of partial shading on CIGS photovoltaic devices: A literature review

Klaas Bakker^{1,a)} , Arthur Weeber², Mirjam Theelen³

¹Delft University of Technology, PVMD, 2628 CD Delft, The Netherlands; and TNO, Energy Transitions—Solliance, 5656 AE Eindhoven, The Netherlands

²Delft University of Technology, PVMD, 2628 CD Delft, The Netherlands; and TNO, Energy Transitions—Solar Energy, 1755 LE Petten, The Netherlands

³TNO, Energy Transitions—Solliance, 5656 AE Eindhoven, The Netherlands

^{a)}Address all correspondence to this author. e-mail: klaas.bakker@solliance.eu

Received: 17 July 2019; accepted: 15 November 2019

Partial shading of Cu(In,Ga)(Se,S)₂ (CIGS) photovoltaic (PV) modules is getting more attention, as is witnessed by the increase in publications on this topic in recent years. This review will give an overview of shading tests executed on CIGS modules and focuses on the more fundamental aspects that are often studied on cells. Generally, CIGS modules display very attractive performance under predictable row-to-row shading. However, potential damage could occur under nonoptimal shading orientations: module output after shading tests could reduce due to the formation of local shunts, often called wormlike defects. The influence of many factors on the formation of these defects, including the internal currents and voltages and the shape and intensity of the shade, will be discussed. This review allows an increased insight in the degradation mechanisms caused by partial shading, which would ultimately lead to the introduction of more shade-tolerant CIGS PV products in the future.

Introduction

Photovoltaic (PV)-based electricity is playing an increasing role as a renewable energy source. Actually, in 2017, the total installed PV capacity was over 400 GWp [1], showing a rapid increase due to a dramatical decrease in cost and increase of efficiency. One of the PV technologies displaying rapid growth are devices based on thin-film Cu(In,Ga)(Se,S)₂ (CIGS) absorbers. These devices contain absorber materials with a direct band gap, therefore allowing solar cell stacks with a thickness of only several microns. Currently, many studies are even working toward solar cells with submicron absorber thicknesses [2]. Moreover, record efficiencies up to 23.35% [3] have been reported, thereby even surpassing efficiencies of multicrystalline silicon solar cells.

The key advantages of CIGS compared to, e.g., crystalline silicon devices include its attractive temperature dependency, a short energy payback time, and advantageous cost projections: due to the reduced amount of required material for thin-film solar cells and the possibility to use low-cost manufacturing techniques, a reduction of costs due to the further scale-up is expected [4].

Moreover, the possibility to deposit fully black PV devices on a large range of substrates, including glass, plastics, and metal foils, allows the usage of the CIGS technology in a large number of new

applications: these include integration into vehicles, astronautics, and portable devices, as well as building integrated PV (BIPV) [4].

A part of the attractive properties of CIGS has an effect on the levelized cost of electricity (LCOE), which is the dominant parameter for successful large-scale market introduction. Lifetime and degradation rates are important factors that influence the LCOE. These factors are, for the LCOE calculations of a PV system, usually based on the warranty provided by the manufacturer [5]. Therefore, PV manufacturers, and their customers, need to be able to accurately predict the lifetime of their products. This is especially important due to the attractiveness of CIGS PV devices for building and product integration, which can lead to an increase in the exposure to uncontrollable stress like partial shading.

Stress loads during partial shading events are 2-fold. First, the redistribution of (electric) power, within the PV module, causes the regions to heat up while other regions cool down. This type of stress is predictable and comparable in nature with other PV technologies. The second stress factor is the influence of the reverse bias potential on the solar cell, which can result in the formation of wormlike defects that are typical for the CIGS technology.

The impact of partial shading strongly depends on the design of the module that is getting exposed. Commercial CIGS modules can be divided into two classes:

- (i) Monolithically interconnected modules, consisting of long, small cells (e.g., 1200 × 5 mm) connected in series by a (laser) interconnection process on an insulating substrate. This approach is chosen for most rigid commercial modules. These modules generally do not contain any mitigation measures to protect the individual cells from any negative effects of partial shading.
- (ii) Modules made up of separated large cells with a current collecting grid in either series or parallel connection. This approach is used by various producers of flexible modules and is in a design very similar to crystalline silicon modules. It allows the use of bypass diodes, so the impact of partial shading can easily be minimized. However, incorporation of bypass diodes in a module comes with a trade-off between added cost and improved electric yield.

The monolithically interconnected modules generally maintain a higher output power when partly shaded [6], especially when it comes to predictable row-to-row shading [7]. In that case, the loss in output power is lower in systems with monolithically integrated modules having vertically oriented narrow cells compared to systems with modules having separated large cells.

However, the reliability impact of partial shading and reverse bias on CIGS is a little-studied subject. From 2015, this topic has gained interest; one of the many reasons could be the announced change in the IEC test protocol [8]. The 2016 version of the IEC 61215 has more stringent requirements on shade tolerability compared to the IEC 61646 which it is replacing. Another reason why this topic has only gained interest in recent years is that the damage done by partial shading is limited when evaluated at standard test conditions. More recent publications revealed that the impact of degradation due to shading effects becomes more pronounced at lower light intensities [9, 10] and the low light performance greatly influences the performance ratio (PR) of a PV system [10].

Origin of reverse bias

Upon shading, local shunts are formed in regions that have been exposed to a reverse bias voltage. To explain the origin of the reverse bias, the reverse bias behavior of a single cell will be described first. Figures 1(a) and 1(b) show the equivalent circuit of a CIGS solar cell and the graphical representation of the position of one cell in a string of cells within a module, respectively. The light-generated current (blue) varies linearly

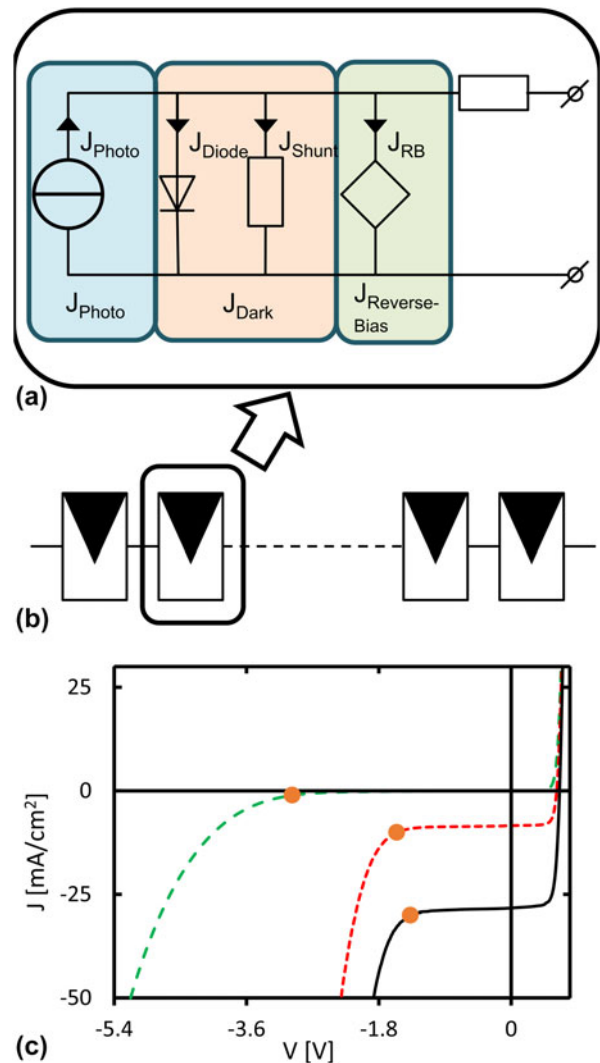


Figure 1: (a) Equivalent circuit of single cell and (b) representation of this cell in a string of cells as found in a PV module. (c) JV characteristic at different illumination intensities of a single cell. The black solid, red dotted, and green dashed lines represent 1 sun, 0.3 sun, and dark conditions, respectively. The transition voltage (V_{tr}) is in each curve marked with an orange dot. Measurements performed on a standard cell, fabricated, and measured at the Solliance facilities.

with light intensity, while the dark current (orange) is the sum of the diode current and the parasitic current through the shunt resistance. The combined contribution of the photo (J_{Photo}) and dark (J_{Dark}) current dominates the JV curve at positive voltages, as can be seen in the JV graph of Fig. 1(c). At negative voltages (reverse bias), there is a third contribution [11] that, besides the shunt resistance, dominates the JV curve, indicated with reverse bias current ($J_{Reverse-Bias}$) in Fig. 1 green. For CIGS solar cells, this element is responsible for the rapid increase in current at negative voltages. The onset of this increase is the transition voltage (V_{tr}) and is indicated with an orange dot in the JV curves in Fig. 1(c). The transition voltage is an indication of the voltage at which the solar cell transits from

an isolating nature to a conducting nature. The reverse characteristic, which is the JV curve at negative voltages, is dominated by the transition and depends strongly on both temperature and illumination. It can be influenced by many parameters which will be discussed in a later section. For better readability, all current and voltage values will be treated as absolute numbers, e.g., a change in the transition voltage from 3 to 2 V will be called a reduction of V_{tr} .

The reverse characteristics of the individual cells in a module determine the internal distribution of voltage and current because a module consists of a string of series connected solar cells. For the example given in Fig. 2, shading is simulated in one cell in a string of ten. The purple dashed line gives the electrical condition at the maximum power point of the constructed JV with nine unshaded and one fully shaded cell. A negative power means that the device is generating energy, while a positive power implies that the device is dissipating energy. Due to the series connection of all cells, the current must be equal in all cells. When the constructed module is operating at the current indicated by the purple dashed line the constructed module is still delivering energy through the external load (negative power in the graph). This energy is supplied by the nine unshaded cells, and the shaded cell is forced to operate at a negative voltage, thus dissipating

the majority of the energy generated by the nine unshaded cells. The magnitude of the dissipation can be altered when the reverse bias characteristic of the cell can be influenced.

Different scenarios for shading tests

In the field, shading can have any arbitrary form or intensity. Since not every thinkable shadow can be tested, Dongaokar et al. [12] introduced several shading scenarios for testing partial shading in monolithically interconnected thin-film modules. The layouts of the shading masks for these scenarios are depicted in Fig. 3. Almost all reported shading tests can be categorized with these mask layouts, except for diagonal shading or shades that mimic a human body.

Besides the shape of the shading mask, also the opacity of the shading mask is an important parameter. Sometimes, a less opaque mask is used to simulate more realistic conditions: a shadow cast by a distant object, during clear sky conditions, blocks approximately 90% of the incident light. Furthermore, shading tests are always executed under an electrical load or at short circuit conditions. Internal currents will flow as a result of externally extracted current from a partial shaded module, which causes internal power flow in the device under test. This can be large enough to cause permanent damage. At open

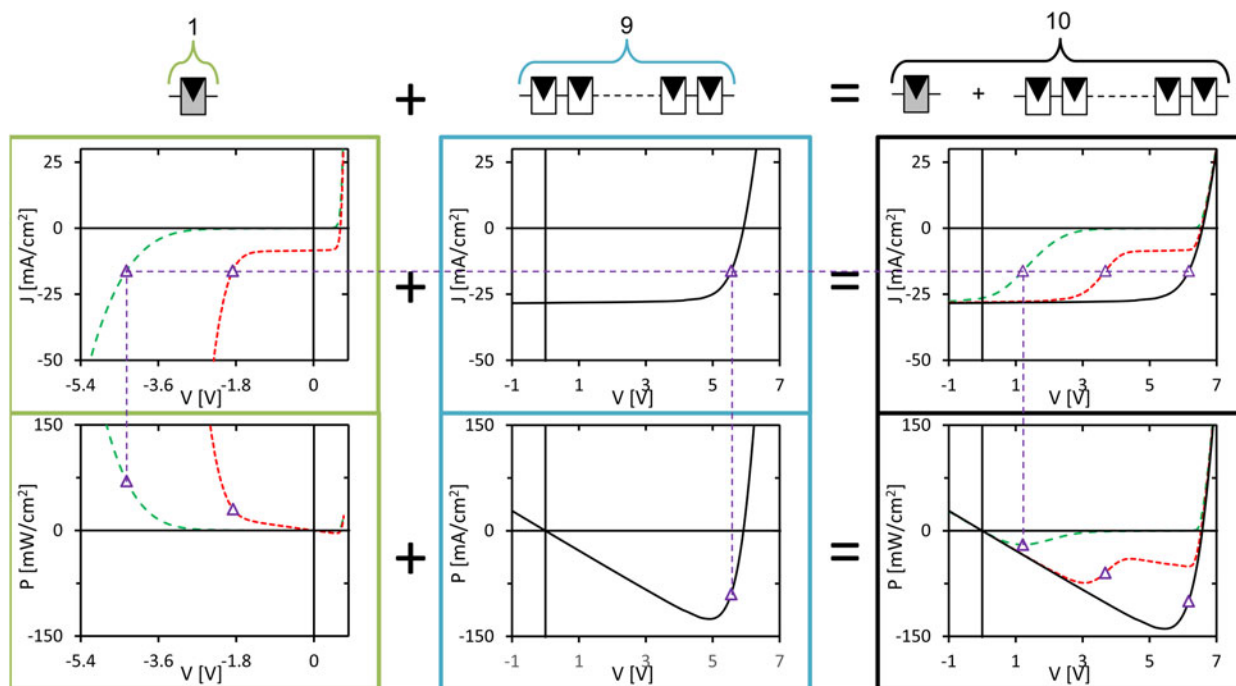


Figure 2: Constructed JV curve representing a module with 9 unshaded cells in series with 1 shaded cell. The graphs at the top are JV curves and the graphs at the bottom are PV curves. On the left the JV and PV curves are plotted of 1 cell at different illumination intensities, the red dotted and green dashed lines represent respectively 0.3 sun and dark conditions. The JV and PV graphs in the middle are constructed from a 1 sun illuminated curve; here, the voltage is multiplied by 9 to get the equivalent JV curve of 9 unshaded cells in series. The graphs on the right are the sum of the graphs of the partly shaded cell and the nine unshaded cells together with (black) an unshaded 10 cell module. The purple symbols represent operating points based on the at the maximum power point current of the constructed module with 1 dark and 9 illuminated cells. The construction is based on JV measurements at different illumination intensities of one-standard cell. This cell was fabricated and characterized at the Solliance facilities in Eindhoven, The Netherlands.

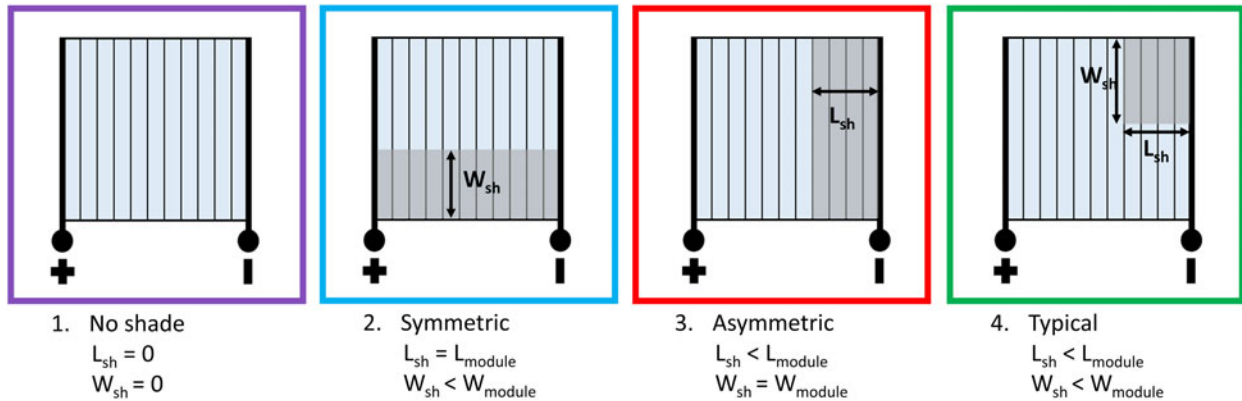


Figure 3: Different shading scenarios as introduced by Donaonkar et al. [12].

TABLE I: Expected local operating parameters for the different shading conditions. Parameters are based on the authors’ interpretation of Refs. 11, 18, and 20.

	No shade		Symmetric		Asymmetric		Typical ($L_{sh} \ll W_{sh}$)		
	Illuminated	Shaded	Illuminated	Shaded	Illuminated	Shaded	Illuminated full cell	Illuminated half cell	Shaded
Current	Imp	NA	Imp	0	Imp	Imp	Imp	>Imp	<Imp
Voltage	Vmp	NA	Vmp	0 till < Vmp	Vmp	RB	Vmp	RB	RB
Temperature	OT	NA	OT	<<OT	OT	<OT	OT	>OT	<OT

Abbreviations used are Imp: current at maximum power point, Vmp: voltage at maximum power point, OT: operating temperature, NA: not applicable, RB: reverse bias.

circuit conditions, no current and power is drawn from the device, so no internal power flow is present.

Local differences in operating parameters are expected for each of the shading scenarios, which are listed in Table I. Scenario 1 represents the normal operating condition with no shade. In case of symmetric shading (scenario 2), power generation of each cell is reduced equally and current and voltage in the shaded regions are uniformly reduced. In the third scenario (asymmetric shading), electrical energy is dissipated in the shaded region because the photo-generated current is forced through the shaded cells. This results in a negative (or reverse) operating voltage of the shaded cells. During typical shading (scenario 4), an additional effect of unequal current distribution acts on the top of the stresses in scenarios 2 and 3. Since the effects are strongest when combined with reverse bias conditions, most shading tests are performed with $L_{sh} \ll W_{sh}$, and this is, unless otherwise stated, the operating condition when referring to the “typical” condition. An example of the temperature distribution for the typical scenario on a module during a field test can be seen in Fig. 4.

Shading tests on modules

Several studies have been published on shading tests performed on monolithically interconnected CIGS modules. A list of them can be found in Table II. Comparing results presented in the existing literature is challenging due to the following reasons:

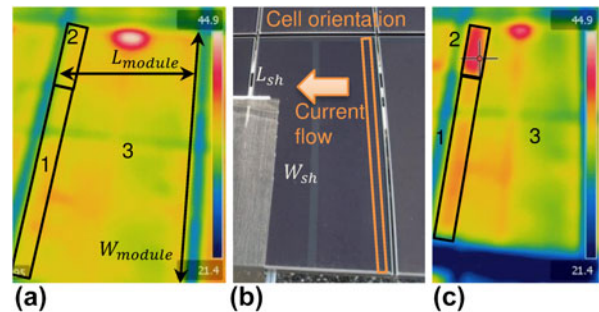


Figure 4: Outdoor measurements of a partial shaded CIGS (Shell Eclipse-80) module. (a) IR picture of module under normal operating condition. The hotspot on top of the module is due to the connectors that caused local heating. (b) Optical picture of module during shading test, with indications of current flow and cell orientation. (c) IR picture directly after the shading test. In (a) and (c) the regions of interest are numbered and indicated. A partly transparent shading mask was applied on region 1. The nonshaded region (Region 2) of the shaded cells exhibit elevated temperatures due to the shading experiment. (Reprinted with permission from Ref. 12.)

- (i) Lack of uniformity in measurement conditions.
- (ii) Most sources report on tests executed on only one module or on a comparison of single modules from different types.
- (iii) Module manufacturers and types are often anonymized.
- (iv) Changes in efficiency and other electrical parameters are not always mentioned.
- (v) Large effect of metastabilities and pre-conditioning on module performance [8]. It is known that light soaking,

TABLE II: List of available literature that describes shading tests on CIGS modules.

First author year reference	Modules Nr + description	Sequence	Mask	Repetitions/ sequence	Relative change ^b in IV parameters ^c	Impact	Remark
...	...	Preconditioning Stress Postconditioning	Scenario Opacity L_{sh}/W_{sh}
Herrmann 2004 [37]	2 Commercial Mi CIS	Light soak Shading indoor ...	Typical 75–100% Worst case/100%	1st determine worst case. 2nd hot spot endurance test	–4.1 and –18.2% η	Uncritical hotspots ^h	Deriving of “old” IEC 61646 standard
Mack 2008 [16]	1 50-cell module	... Shading indoor Light soak	Typical 100% 1 cell/100%	...	–6% η loss in V_{oc} and FF	...	Improvement with light soaking
Dongaonkar 2013 [12]	1 Commercial Mi	...	Assy–Typ 73% 19 cm/75%	Only thermal results
Silverman 2015 [18]	1 Commercial Mi	... Shading outdoor ...	Typical 90% 10 cells/50%	Heating from localized shunting
Silverman 2015 [8]	3 Commercial Mi	Light soak @mpp Shading indoor Light soak @mpp	Typical 90% Worst case/90%	New mask position till 50% of module was stressed	–4.7, –6.5, –10.5% η	Local shunts in EL. Visible defects	–4.2, –6.1, –11.4 η after light soaking. New shunts after subsequent test
Wendlandt 2016 [38]	3 Commercial Mi	Light soak Shading indoor ...	10 different 100% ...	10 scenarios on each module	...	Uncritical hotspots ^h visible defects	Only studied hotspots
Silverman 2016 [17]	1 Commercial Mi CIGS + CdTe ⁽¹⁾	Light soak @mpp Shading outdoor Light soak @mpp	Typical 100% @ 1 m ^f 75 mm/90%	...	–5% η	Local shunts in EL wormlike (serpentine) defects	–7% η after light soak
Silverman 2016 [17]	6 Commercial Mi CIGS + CdTe ⁽¹⁾	Light soak @mpp Shading indoor Light soak @mpp	Typical 90% Worst case/90%	New mask position till 50% of module was stressed	–3 to –11% η	Local shunts in EL	–4 to –14% η after light soak (2 out of 6 improved)
Lee 2016 [27]	3 Commercial Mi	... Shading indoor ...	Typical 100% 0–100%/100%	10 times, progressing Cover from 0 to 100%	–2.3% η –1.8% FF	Local shunts in EL Wormlike defects	Only IV data for 1 out of 3 modules
Silverman 2017 [14]	4 Commercial Mi CIGS + CdTe ⁽¹⁾	Light soak @mpp Shading outdoors Light soak @mpp	Humans + cleaning tools ^g	>6	–25% $I_{mp}/$ I_{sc} (worst module)	Local shunts in EL	New shunts formed every repetition
Tzikas 2017 [15]	6 Commercial Mi 1 Commercial C	... Shading indoor ... ^d	Symmetric + asymmetric 100% 0–100%/0–100%	Progressing 5% increment cover from 0 to 100%	–2 to –8% η	Local shunts in EL Wormlike defects	Improvement after dark storage
Wendlandt 2018 [10]	1 Commercial Mi	... ^e Shading indoor ...	Typical 10%/100% 100%	10 times new mask position	+0.7% η	Local shunts in EL	–15.9% η at 100 W/m ²

(continued)

TABLE II: List of available literature that describes shading tests on CIGS modules. (continued)

Silverman 2018 [9]	7 Commercial Mi CIGS + CdTe ^a	Light soak @mpp Shading outdoor Light soak @mpp	Human body and cleaning tool 90 and 100% NA	33 times 7 different tests, new module each test	-2% to -27% η	Local shunts in EL	Bigger losses at lower intensities
-----------------------	--	---	---	---	-----------------------	-----------------------	---------------------------------------

Abbreviations used: L_{sh} and W_{sh} : length and width of shading mask, respectively, according to Fig. 3, Mi: monolithically interconnected, C: nonmonolithically interconnected, T_{mod} : module temperature, CIS: CuInSe₂, I_{sc} : short circuit current, Imp: current at maximum power point, η : efficiency, V_{oc} : open circuit voltage, FF: fill factor.

^aData were anonymized in such a way that the distinction between CIGS and CdTe could not be made.

^bLoss in parameters are relative to before application of stress. For example -10% η means that a module went from an efficiency of 20% before the test to an efficiency of 18% after the test.

^cIV parameters at standard test conditions. If also low light measurements were performed, this is indicated in the last column.

^dTzikas et al. [15] also measured IV after several weeks of dark storage.

^eWendlandt et al. [10] started with stabilized modules.

^fSilverman et al. [17] used a 100% opaque mask at a distance of 1 m outdoor that was moved in such a way that the shadow passed over the full width of the module in 20 s.

^gSilverman et al. [14], tested the influence of real humans and cleaning tools (no artificial masks).

^hIn c-Si modules often breakage of glass and melting of encapsulant has been observed; therefore, a noncritical hotspot does not generate sufficient heat to break the glass or melt the encapsulant.

electrical biases, and module temperature can temporarily influence the module performance [13]. Therefore, separation of the permanent effects of the partial shading tests and the temporary effects, which are often independent of the partial shading, is very complicated.

Besides the challenges, the main observation is that after shading tests, modules displayed a reduced efficiency, which is accompanied by the formation of local shunts. In all publications from 2015 till present (Table II), local shunts are described, which are commonly linked to the following observations:

- (i) Reduction of module efficiency due to a reduced fill factor, associated with local shunts.
- (ii) The formation of shunts is a very fast process, and hence, defects can form within one 10-ms single flash IV measurement [10] or after several 100-ms flashes [8].
- (iii) The occurrence of shunts does not stop with consecutive measurements, the damage adds up after each new stress exposure [9, 14]. The impact on module performance can, therefore, become severe, even though the individual effects of stress exposure are sometimes small.
- (iv) The defects causing the shunts are often referred to as wormlike defect, due to their distinct visual appearance. An example of the typical appearance of wormlike defects after a shading test can be found in Fig. 5. More information on these defects is presented in a later section.
- (v) The wormlike defects form in the region where a reverse bias voltage was present.

Another observation is that shading test lead to an initial change in performance, which is not stable over time. Some

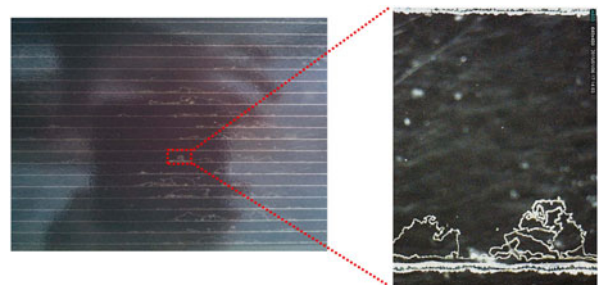


Figure 5: Pictures of wormlike defects in a CIGS module after shading stress test. (Reprinted with permission from Ref. 27.)

authors observed recovery after dark storage [15] or light soaking [16], but also mixed results were found with both improving and degrading modules after light stabilization treatment [8, 17].

Thermoelectrical models on CIGS cells and modules

To estimate the stress loads during partial shading events, it is important to predict the internal voltage, current, and temperature profiles. Thermoelectrical modeling can, therefore, be used to explain the temperature differences during shading events, as would occur in the field (Fig. 4). Specific models that are developed for CIGS devices have to take into account the nonlinear dependency of the reverse curve on illumination. This mechanism is responsible for the internal electrical current flow that is preferential in the illuminated area [18]. The following thermoelectrical models and how they included the light dependency for CIGS devices have been published:

- (i) Sun et al. [11] introduced the Poole-Frenkel mechanism to account for the light dependency of the reverse

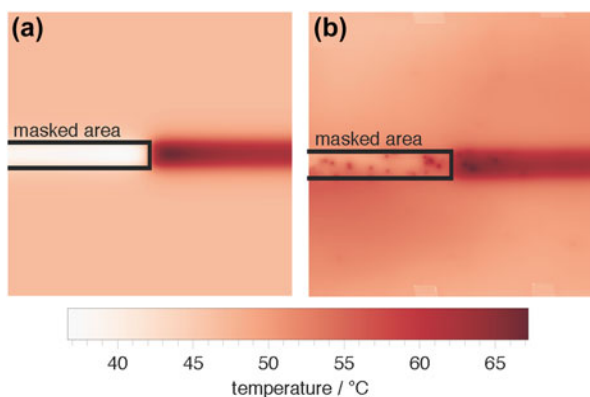


Figure 6: Simulated and measured maps of the back of the module temperature. The area inside the black line is the shaded area. (a) Simulation results of 100 cells in a 0.5×0.5 m module. (b) Measurement of 0.6×0.6 m portion of a larger commercial module. (Reprinted with permission from Ref. 18.)

characteristic. The model uses a 2D SPICE simulation. The Poole–Frenkel principle was verified with the aid of cell measurements from another publication [19].

- (ii) Silverman et al. [18], used the Poole–Frenkel mechanism introduced by Sun et al. [11]. They validated the thermoelectrical model with temperature measurements on a commercial module. The model utilizes commercial Finite Element Analyses software.
- (iii) Carolus et al. [20], also used a thermoelectrical 2D SPICE model. The light dependency is accounted for by the use of measured JV curve both in the dark and under illumination. Verification of their model is a work in progress that has not yet been published.

Predictions do not always match reality as was shown by Silverman et al. [18] who compared the modeled and actual temperature data (Fig. 6). The model correctly predicted an increase in temperature for the noncovered parts of the partly masked cells. However, their measurements showed small hotspots in both the covered and noncovered parts of the partly masked cells. These hotspots originate from already existing local shunts as well as the formation of new reverse bias induced defects. This type of defects has been successfully predicted by Nardone et al. [21], who included local weak spots in their model. These weak spots consumed all current in the shaded cells, causing local heating.

Reverse bias induced defects

In a module, the reverse bias induced defects act as local shunts and are often referred to as wormlike defects due to their distinct visual appearance. The first observation in 2007 was by van Dyk et al. [22]; however, they did not name them wormlike defects or linked them with the exposure to reverse bias. Introduction of the term wormlike defect came from Westin

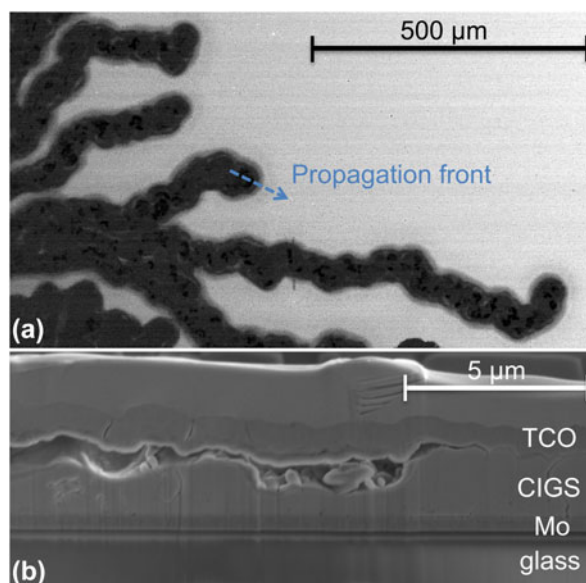


Figure 7: (a) EBIC picture of wormlike defect. Brighter colors represent more efficient current collection. The wormlike defect appears darker in this image, meaning that the defect has completely different electronic properties. (b) Cross-section of wormlike defect prepared with focused ion beam (FIB). Large voids have been formed at the TCO–CIGS interface. (Reprinted with permission from Ref. 25.)

et al. [23] in 2009. Some descriptions that have been given on the origin and nature of the wormlike defects are follows:

- (i) Formation has been observed as being a moving hotspot that moves toward the P1 scribe, while propagation along the P1 scribe is also observed [23, 24, 25, 26].
- (ii) The origin is often an already existing weak spot like a small shunt [24, 25, 26].
- (iii) The absorber material has changed into a very porous structure [23, 25, 27] leading to changes in both composition and electronic properties. An example of the changed electronic properties is shown in the electron beam induced current (EBIC) image of Fig. 7(a).
- (iv) Large voids have been found at the interface of the transparent conductive oxide (TCO) and the CIGS material, as can be seen in Fig. 7(b). Lifting the TCO layer gives the signature appearance [23, 25].
- (v) The composition inside the defects has changed; zinc from the aluminum-doped zinc oxide TCO has been found to migrate into the CIGS absorber, while copper migrated toward the back contact. Brighter areas that have been found in SEM cross-section are believed to be phase segregations [23].

Regardless of these studies, many questions about the origin and propagation mechanisms of these wormlike defects still exist. Explanations using thermoelectrical models are contradictory.

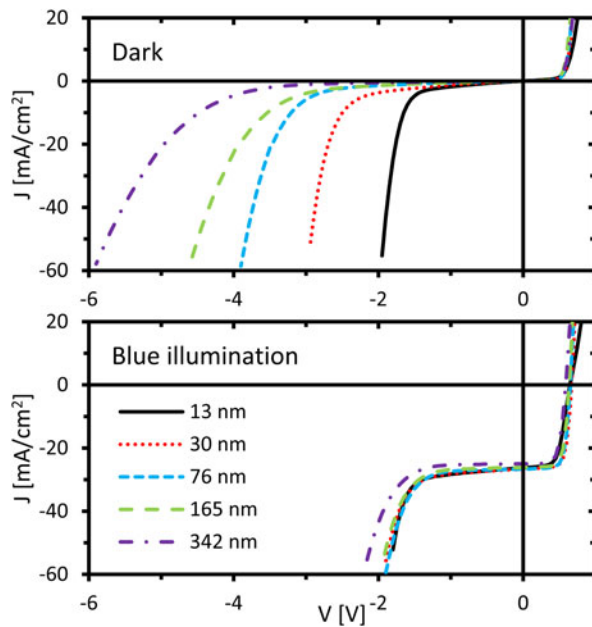


Figure 8: Influence of buffer layer thickness on both dark and (blue) illuminated JV curves. The top graph shows JV measurements in the dark with decreasing transition voltage with increasing buffer layer thickness (thickness increase from black solid to purple dashed dotted curve). Bottom graph shows JV measurements of the same cells with blue illumination. (Reprinted with permission from Ref. 19.)

Richter et al. [28] concluded that neither diode-like defects nor ohmic shunts could generate sufficient heat to cause irreversible damage. Nardone et al. [21] on the other hand calculated that the current density in a local weak spot can reach approximately 10^8 A/m [2], with accompanying peak temperatures above 900 K, enough to cause permanent material damage.

Experimental evidence exists that the wormlike defects originate in local weak spots like shunts [24, 25, 26]. However, Richter et al. [29] showed by using statistical analyses that the formation of wormlike defects is likely driven by an electric field rather than high local currents associated with local defects. The results from Richter et al. [29] are in line with the results from Puttnins et al. [30], who found a lower chance of forming wormlike defects when a thicker TCO was used.

Reverse characteristic of single cells

One of the means to prevent reverse bias induced defects from forming is to limit the reverse bias voltage over a cell. This can be achieved by alternating the reverse characteristic in such a way that it acts as a build-in bypass diode. This requires a good understanding of the mechanisms behind the transition. Therefore, several studies have been performed on the reverse characteristic [16, 17, 18, 19, 30, 31, 32, 33].

A uniform description of the reverse characteristic is needed to be able to reliably compare studies from different sources. Unfortunately, the shape of the reverse characteristic

has not been described thoroughly, which is in contrast with the forward region of the JV curve. Here, the shape of the curve can be described by the combination of 5 parameters (V_{oc} , I_{sc} , FF, R_{shunt} , and R_{series}). The shape of the reverse characteristic seems more complex and is less studied. Often, one characteristic point on the reverse bias curve is used to compare samples within a study. The transition voltage is one of these points used to compare reverse characteristics. Two different approaches for the determination of the transition voltage have been published [31, 32]. A more empiric method to compare the shapes of different reverse characteristics is to use the voltage needed to drive either a fixed current [17] (30 mA/cm² in the dark and 70 mA/cm² under illumination) or the photocurrent [16].

Several publications have reported on the influence of external conditions, like illumination intensity, spectrum of the light source, and temperature, on the reverse characteristic. The reported trends include the following:

- (i) A shift in transition voltages with illumination intensity [16, 18, 31]: a higher light intensity leads to a reduction in V_{tr} .
- (ii) Influence of the spectrum of the illumination source on the transition voltage. Several sources [16, 19, 31] reported that high energetic blue illumination reduces the transition voltage, while illumination with low energetic (red) light more resembled the behavior in the dark.
- (iii) The transition voltage increases when the temperature is reduced [19, 31]. However, there seems to be a local maximum in the transition voltage around 200 K which depends on illumination wavelength [31]. Below this temperature, the transition voltage reduces again.

Besides external factors, the composition of the solar cell also influences the reverse characteristics; some reported compositional influences are as follows:

- (i) Effects of the buffer layer;
 - (a) The buffer layer thickness influences the transition voltage, a thicker buffer layer leads to a higher transition voltage in the dark [19, 30]. This is, however, not the case when illuminated with blue light [19], as is shown in Fig. 8 for cells with a ZnSnO (ZTO) buffer layer with varying thickness.
 - (b) No influence of the buffer layer material. Cells with CdS and ZTO layers show the same behavior both in the dark [19, 32] and with blue illumination [19].
- (ii) A higher sodium concentration in the CIGS layer reduces the transition voltage [31, 33].
- (iii) The influence of the TCO layer thickness on the reverse characteristic is very small; however, a thicker TCO layer dramatically improved the survival rate of the cells from 25 to 75% [30].

- (iv) The reverse characteristic reduces when the absorber layer thickness is reduced [17].

The observed trends are the basis of speculation on the mechanism behind the transition. Based on similarities with traditional semiconductor physics, the main mechanisms discussed are impact ionization (avalanche effect) or tunneling (Zener effect). Although also other tunneling mechanism (Poole–Frenkel and Fowler–Nordheim) have been considered specifically for CIGS devices. The suggested mechanisms in chronological order of publication are as follows:

- (i) Mack et al. [16] concluded that the transition in the dark could be caused by either tunneling or avalanche currents, and the process is likely assisted by metastable interface charges.
- (ii) Szaniawski et al. [19] concluded that under illumination, tunneling is the exclusive mechanism behind the transition. However, in the dark, it could be either tunneling or a combination of tunneling and avalanching.
- (iii) Puttnins et al. [31] argued that in dark, it could be either tunneling or a combination of tunneling and avalanching.
- (iv) Silverman et al. [18] together with Sun et al. [11] introduced the Poole–Frenkel mechanism to account for the observed differences between dark and illumination behavior.
- (v) Nardone et al. [34] showed with semiconductor physics device simulations that the conventional mechanisms (including Poole–Frenkel) cannot adequately describe the reverse characteristic of CIGS cells.
- (vi) Szaniawski et al. [32] introduced the Fowler–Nordheim tunneling as the dominant mechanism in the dark.

Over time, the more traditional Zener and avalanche mechanisms have been replaced by more complicated tunneling mechanisms. However, the mechanisms proposed do not fully explain the observed difference between the behavior under illumination and in the dark. The key in understanding the reverse characteristic of CIGS cells would be a mechanism that explains the discrepancy between light and dark. The Poole–Frenkel mechanism [11, 18] could provide such an explanation. However, it was proven both experimentally [32] and theoretically [34] that the Poole–Frenkel mechanism is probably not responsible for the transition in the dark. So, despite all the efforts, there is still more research needed to fully understand the mechanism behind the reverse characteristic.

Nonpermanent effects

While the formation of wormlike defects likely has the largest effect on device performance, various other effects have also been observed on single cells or small research modules:

- (i) Mack et al. (2008) [16], observed metastabilities caused by illumination and annealing at 160 °C in the dark. Light soaking and annealing reduces and increases the transition voltage, respectively.
- (ii) Westin et al. (2008) [23] observed degradation of V_{oc} and FF after combined exposure of cells to illumination and reverse bias. This was in contrast to cells that were only exposed to reverse bias in the dark, which only showed a reduction of the FF. They also reported that degradation of the V_{oc} could be recovered by light soaking.
- (iii) Szaniawski et al. (2013) [19] observed a very slow response of the current to changes in illumination for cells held at a constant negative voltage. In their study, it could take up to 5 min for the current to reach an equilibrium state after changes in illumination were applied.
- (iv) Szaniawski et al. (2017) [32] observed that the reverse characteristic was shifting when repeating reverse JV measurements. They also described an increase in current over time when a cell is kept at a fixed negative voltage in the dark.
- (v) Mortazavi et al. (2017) [35] observed a decrease in JV parameters for cells after a short (1 min) exposure to reverse bias voltages larger than 2 V. They also reported severe damage for cells after long (1 h) exposure to reverse voltages of 1.5 and 2 V, which could partly be recovered by light soaking.
- (vi) Theelen et al. (2016) [36] observed that during combined damp heat and illumination conditions, cells that were kept at a negative bias degraded more rapidly than the cells held at V_{oc} , J_{sc} , or maximum power point over a period of 200 h.

Conclusions

The largest reliability impact of partial shading of CIGS modules is the formation of reverse bias induced wormlike defects. The appearance and morphology of these defects have been studied; nonetheless, the origin and exact mechanisms behind the formation and propagation remain unclear. Wormlike defects have been found in most modules that have been exposed to shading tests. It has to be mentioned that there was a change in the IEC norm, and it could be expected that newer products that enter the market will be much more shade-tolerant as it is required by this new IEC regulations. On top of that, both the published and ongoing research in this field will also contribute to the introduction of more shade-tolerant CIGS PV products.

Acknowledgments

The authors would like to thank Sourabh Dongaonkar, Timothy Silverman, Elizabeth Palmiotti, Steve Johnston, and

Piotr Szaniawski for providing the original data files used to reproduce their figures.

This work is supported by the “Netherlands Enterprise Agency” (RVO) and the Dutch TopTeam Energy via the projects: “Building Integrated PhotoVoltaic Panels on Demand—in The Netherlands” with grant number TEID215005 and “Performance and Electroluminescence Analysis on Reliability and Lifetime of Thin-Film Photovoltaics” with grant number TEUE116203. Furthermore, the Early Research Program “Sustainability & Reliability for solar and other (opto-)electronic thin-film devices” from TNO is also acknowledged for funding.

References

- D.S. Philips and W. Warmuth:** *Fraunhofer ISE: Photovoltaics Report*, Updated: 14 March 2019 (2019).
- G. Birant, J. de Wild, M. Meuris, J. Poortmans, and B. Vermang:** Dielectric-based rear surface passivation approaches for Cu(In,Ga)Se₂ solar cells—A review. *Appl. Sci.* **9**, 677 (2019).
- M.A. Green, E.D. Dunlop, D.H. Levi, J. Hohl-Ebinger, M. Yoshita, and A.W.Y. Ho-Baillie:** Solar cell efficiency tables (version 54). *Prog. Photovolt. Res. Appl.* **27**, 565 (2019).
- T. Feurer, P. Reinhard, E. Avancini, B. Bissig, J. Löckinger, P. Fuchs, R. Carron, T.P. Weiss, J. Perrenoud, S. Stutterheim, S. Buecheler, and A.N. Tiwari:** Progress in thin film CIGS photovoltaics—Research and development, manufacturing, and applications. *Prog. Photovolt. Res. Appl.* **25**, 645 (2017).
- K. Branker, M.J.M. Pathak, and J.M. Pearce:** A review of solar photovoltaic leveled cost of electricity. *Renew. Sustain. Energy Rev.* **15**, 4470 (2011).
- H. Ziar, B. Asaei, S. Farhangi, M. Korevaar, O. Isabella, and M. Zeman:** Quantification of shading tolerability for photovoltaic modules. *IEEE J. Photovolt.* **7**, 1390 (2017).
- K. Brecl and M. Topić:** Self-shading losses of fixed free-standing PV arrays. *Renewable Energy* **36**, 3211 (2011).
- T.J. Silverman, M.G. Deceglie, C. Deline, and S. Kurtz:** *SPIE Optics + Photonics for Sustainable Energy* (2015); p. 95630F.
- T.J. Silverman and I. Repins:** 2018 *IEEE 7th World Conference on Photovoltaic Energy Conversion (A Joint Conference of 45th IEEE PVSC, 28th PVSEC, & 34th EU PVSEC)* (IEEE, Piscataway, 2018); pp. 3932–3937.
- S. Wendlandt and L. Podlowski:** 35th *Photovoltaic Solar Energy Conference and Exhibition* (WIP Renewable Energies, Munich, 2018); pp. 1230–1235.
- X. Sun, J. Raguse, R. Garris, C. Deline, T. Silverman, and M.A. Alam:** 2015 *IEEE 42nd Photovoltaic Specialist Conference* (IEEE, Piscataway, 2015); pp. 1–6.
- S. Dongaonkar, C. Deline, and M.A. Alam:** Performance and reliability implications of two-dimensional shading in monolithic thin-film photovoltaic modules. *IEEE J. Photovolt.* **3**, 1367 (2013).
- M. Gostein and L. Dunn:** 2011 37th *IEEE Photovoltaic Specialists Conference* (IEEE, Piscataway, 2011); pp. 003126–003131.
- T.J. Silverman and R. Ingrid:** 33rd *European Photovoltaic Solar Energy Conference and Exhibition* (WIP Renewable Energies, Munich, 2017); pp. 1422–1426.
- C. Tzikas, G. Gomez, M. van den Donker, K. Bakker, A.H.M. Smets, and W. Folkerts:** 33rd *European Photovoltaic Solar Energy Conference and Exhibition* (WIP Renewable Energies, Munich, 2017); pp. 1593–1596.
- P. Mack, T. Walter, R. Kniese, D. Hariskos, and R. Schäffler:** 23rd *European Photovoltaic Solar Energy Conference and Exhibition* (WIP Renewable Energies, Munich, 2008); pp. 2156–2159.
- T.J. Silverman, L. Mansfield, I. Repins, and S. Kurtz:** Damage in monolithic thin-film photovoltaic modules due to partial shade. *IEEE J. Photovolt.* **6**, 1333 (2016).
- T.J. Silverman, M.G. Deceglie, X. Sun, R.L. Garris, M.A. Alam, C. Deline, and S. Kurtz:** Thermal and electrical effects of partial shade in monolithic thin-film photovoltaic modules. *IEEE J. Photovolt.* **5**, 1742 (2015).
- P. Szaniawski, J. Lindahl, T. Törndahl, U. Zimmermann, and M. Edoff:** Light-enhanced reverse breakdown in Cu(In,Ga)Se₂ solar cells. *Thin Solid Films* **535**, 326 (2013).
- M.D.J. Carolus, Z. Purohit, T. Vandenberg, M. Meuris, and B. Tripathi:** 35th *European Photovoltaic Solar Energy Conference and Exhibition* (WIP Renewable Energies, Munich, 2018); pp. 1343–1345.
- M. Nardone, S. Dahal, and J.M. Waddle:** Shading-induced failure in thin-film photovoltaic modules: Electrothermal simulation with nonuniformities. *Sol. Energy* **139**, 381 (2016).
- E.E. van Dyk, C. Radue, and A.R. Gxasheka:** Characterization of Cu(In,Ga)Se₂ photovoltaic modules. *Thin Solid Films* **515**, 6196 (2007).
- P.O. Westin, U. Zimmermann, L. Stolt, and M. Edoff:** 24th *European Photovoltaic Solar Energy Conference* (WIP Renewable Energies, Munich, 2009); pp. 2967–2970.
- S. Johnston, E. Palmiotti, A. Gerber, H. Guthrey, L. Mansfield, T.J. Silverman, M. Al-Jassim, and A. Rockett:** 2017 *IEEE Photovoltaic Specialists Conference* (IEEE, Piscataway, 2017); pp. 1400–1404.
- E. Palmiotti, S. Johnston, A. Gerber, H. Guthrey, A. Rockett, L. Mansfield, T.J. Silverman, and M. Al-Jassim:** Identification and analysis of partial shading breakdown sites in CuIn_xGa_(1-x)Se₂ modules. *Sol. Energy* **161**, 1 (2018).
- S. Johnston, D. Sulas, E. Palmiotti, A. Gerber, H. Guthrey, J. Liu, L. Mansfield, T.J. Silverman, A. Rockett, and M. Al-Jassim:** 2018 *IEEE 7th World Conference on Photovoltaic Energy Conversion (WCPEC) (A Joint Conference of 45th IEEE PVSC, 28th PVSEC & 34th EU PVSEC)* (IEEE, Piscataway, 2018); pp. 1897–1901.
- J.E. Lee, S. Bae, W. Oh, H. Park, S.M. Kim, D. Lee, J. Nam, C. Bin Mo, D. Kim, J. Yang, Y. Kang, H. Lee, and D. Kim:**

- Investigation of damage caused by partial shading of $\text{CuIn}_x\text{Ga}_{(1-x)}\text{Se}_2$ photovoltaic modules with bypass diodes. *Prog. Photovolt. Res. Appl.* **24**, 1035 (2016).
28. **M. Richter, J. Neerken, and J. Parisi:** *32nd European Photovoltaic Solar Energy Conference and Exhibition* (WIP Renewable Energies, Munich, 2016); pp. 1116–1119.
 29. **J.P.M. Richter and M. Vrengor:** *33rd European Photovoltaic Solar Energy Conference and Exhibition* (WIP Renewable Energies, Munich, 2017); pp. 1017–1019.
 30. **S. Puttnins, S. Jander, K. Pelz, S. Heinker, F. Daume, A. Rahm, A. Braun, and M. Grundmann:** *26th European Photovoltaic Solar Energy Conference and Exhibition* (WIP Renewable Energies, Munich, 2011); pp. 2432–2434.
 31. **S. Puttnins, S. Jander, A. Wehrmann, G. Benndorf, M. Stölzel, A. Müller, H. von Wenckstern, F. Daume, A. Rahm, and M. Grundmann:** Breakdown characteristics of flexible $\text{Cu}(\text{In,Ga})\text{Se}_2$ solar cells. *Sol. Energy Mater. Sol. Cells* **120**, 506 (2014).
 32. **P. Szaniawski, P. Zabierowski, J. Olsson, U. Zimmermann, and M. Edoff:** Advancing the understanding of reverse breakdown in $\text{Cu}(\text{In,Ga})\text{Se}_2$ solar cells. *IEEE J. Photovolt.* **7**, 1136 (2017).
 33. **S. Puttnins, M. Purfurst, M. Hartung, H.K. Lee, F. Daume, L. Hartmann, A. Rahm, A. Braun, and M. Grundmann:** *27th European Photovoltaic Solar Energy Conference and Exhibition* (WIP Renewable Energies, Munich, 2012); pp. 2219–2221.
 34. **M. Nardone and S. Dahal:** Anomalous reverse breakdown of CIGS devices: Theory and simulation. *MRS Adv.* **2**, 3163 (2017).
 35. **S. Mortazavi, K. Bakker, J. Carolus, M. Daenen, G. de Amorim Soares, H. Steijvers, A. Weeber, and M. Theelen:** *2017 IEEE 44th Photovoltaic Specialist Conference* (IEEE, Piscataway, 2017); pp. 2875–2880.
 36. **M. Theelen, H. Steijvers, K. Bakker, J. Vink, S. Mortazavi, A. Mulder, N. Barreau, D. Roosen, and E. Haverkamp:** *2016 IEEE 43rd Photovoltaic Specialists Conference* (IEEE, Piscataway, 2016); pp. 0929–0934.
 37. **W. Herrmann and M.C. Alonso:** *19th EUPVSEC* (WIP Renewable Energies, Munich, 2004).
 38. **S. Wendlandt, S. Berendes, T. Weber, J. Berghold, S. Krauter, and P. Grunow:** *32nd EUPVSEC* (WIP Renewable Energies, Munich, 2016); pp. 2270–2276.